$MoTe_2$ Under the Electron Beam

April 26, 2019 · salve-project.de/newspress/mote2-under-the-electron-beam.html

April 26, 2019 – New point and line defects have been revealed in single-layer $MoTe_2$ under the electron beam. With the C_c/C_s-corrected SALVE microscope at 40 kV, researchers from Ulm, Dresden and Aalto followed how tellurium vacancies cluster into tetravacancies and trefoils, line up into vacancy lines and finally form inversion domains and islands of the metallic 1T′ phase. First-principles calculations showed that some of the defects carry magnetic moments and that vacancy lines act as metallic quantum wires, which may make $MoTe_2$ a platform for quantum devices.

A perfect crystal is predictable, and for many future devices that is exactly its limitation. Missing atoms, rows of vacancies and boundaries between mirror-image domains can give a semiconductor sheet new electronic, magnetic and optical functions, provided that one knows how such defects form and what they do. Scientists from Ulm University, the Helmholtz-Zentrum Dresden-Rossendorf and Aalto University in Finland have now followed, atom by atom, how defects arise and evolve in single-layer molybdenum ditelluride ($MoTe_2$) under the electron beam. They imaged the material with the C_c/C_s-corrected SALVE microscope at 40 kV[1]–[3], which both creates and resolves the defects, and used first-principles calculations to work out their electronic and magnetic properties. Several of the defects had never been observed before, and some of them carry a magnetic moment, which sets the stage for future quantum devices.

Defects as building blocks

Transition metal dichalcogenides (TMDs) such as $MoTe_2$ are layered materials that, depending on their elements, can be insulators, semiconductors, metals, superconductors or show charge density waves[4]–[6]. Single sheets can be exfoliated[4] or grown by chemical vapor deposition[7], and they promise numerous practical applications[8]. In a transmission electron microscope (TEM), they can be modified and imaged at the same time, with the electron beam serving both as an imaging tool and as a means to change the material[9]–[13]. $MoTe_2$ is a particularly interesting case: its semiconducting 2H phase and its metallic 1T′ phase differ in energy by only about 31 meV per formula unit.

Defects and their agglomeration can drastically change the properties of these materials[5],[8],[14], for example by creating catalytically active centers[15]. Mirror twin boundaries (MTBs), the borders of inversion domains in which the lattice is turned by 180°[16]–[18], can form one-dimensional metallic quantum objects inside a semiconducting matrix[19]. Yet it was not clear what role point defects play in MTB formation or how mechanical strain affects it. The exact structure and direction of line defects can differ widely[20],[21], and the reason remained elusive, partly because contrast and resolution are limited in conventional C_s-corrected TEMs.

Imaging at 40 kV

The researchers therefore used a microscope corrected for both spherical (C_s) and chromatic (C_c) aberration. The SALVE microscope reaches a resolution of 0.9 Å at 40 kV and records fully atomic-position-corrected images within about one second over a large field of view[2]. In such images, a single missing tellurium atom can be told apart from two missing ones (Fig. 1): a Te column with one atom left is still slightly brighter than a neighboring Mo atom, while a column Te divacancy, in which both stacked Te atoms are gone, shows almost no signal. The DFT calculations gave formation energies of 4.87 eV for a single Te vacancy and 4.46 eV per Te atom for a column divacancy. Mo vacancies cost 10.45 eV, which agrees with the observation that only Te vacancies and related defects occurred.

Direct knock-on damage should not occur at 40 kV, because the Te and Mo atoms are heavy[22]: the electrons can transfer at most 0.72 eV to a Te atom and 0.95 eV to a Mo atom, far below the formation energies, and actual displacement thresholds are even higher[22]. Still, the vacancy concentration grew under the beam. The exact mechanism is not known, but beam-induced chemical etching by fragments of water and other molecules on the sample surface is a likely cause[23]. How the samples were prepared and imaged is described in the box below (Fig. 2).

SALVE: imaging $MoTe_2$ at 40 kV

$MoTe_2$ monolayers were exfoliated with adhesive tape onto silicon wafers with 90 nm of oxide, identified in the optical microscope by their contrast and transferred onto Quantifoil TEM grids; the oxide was etched away with potassium hydroxide. Some regions stayed contaminated, but enough clean areas remained.

The SALVE microscope was operated at 40 kV with C_c and C_s between −10 and −20 µm, at a column vacuum of about 10^{-5} Pa. Images were recorded on a 4k × 4k camera with 1 s exposure at dose rates of about 10^6 electrons per nm^2 and second. In a series over the same area, the vacancy density rose from about 0.17 to 0.27 vacancies per nm^2 after a total dose of about 1.2×10^9 electrons per nm^2, and tetravacancies appeared next to the single and column vacancies (Fig. 2).

The TEM mode allows fast acquisition over a large field of view, so the dynamics of point defects and their surroundings can be followed in detail. Earlier work with scanning TEM (STEM) had also found Te migration and rotational defects in $MoTe_2$, but the defects produced in TEM mode look somewhat different.

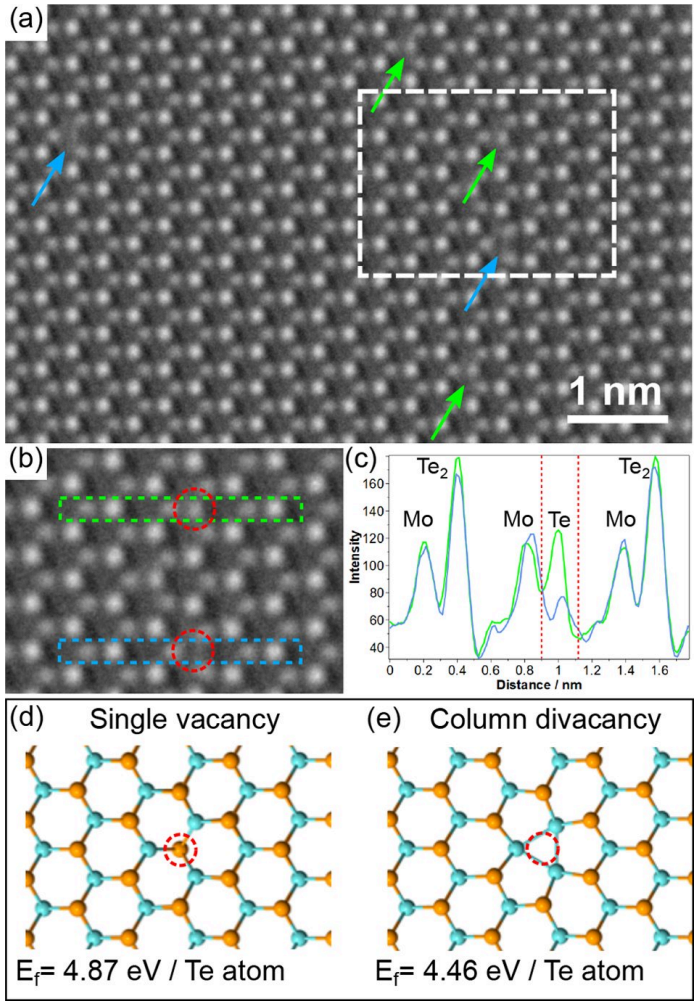

Fig. 1: Te vacancies at 40 kV.

Vacancies that team up

The beam also produced more complex defects, in which several atoms are missing (Fig. 3). The team called them “extended point defects”, as they lie between true point defects, such as single vacancies, and extended structures, such as vacancy lines of arbitrary length. They start with two column Te divacancies. Two Te atoms migrate into the center and form a symmetric defect, tetravacancy I. This configuration is metastable: within 21 s it distorted into the more stable tetravacancy II (Fig. 3b). After further irradiation and the loss of another Te_2 column, a symmetric trefoil-like defect, trefoil I, appeared 271 s later (Fig. 3c). Tetravacancies I and II had never been observed before. Image simulations and further defect variants are shown in the box below (Figs. 4, 5 and 6).

Extended point defects in simulation

HRTEM image simulations based on the DFT structures reproduce tetravacancy I, tetravacancy II and trefoil I at the sampling of the experimental images (Fig. 4). The faint, blurred contrast of the Mo atoms around the central Te_2 column in the experiment, which is absent in the simulation, may come from vibrating Mo atoms and points to tetravacancy I being metastable.

A bond rotation can turn the observed structures into other variants: tetravacancy III and the distorted tetravacancy IV (Fig. 5), and trefoil II (Fig. 6). These variants have higher formation energies, in line with the fact that they did not appear in the experiment.

Quantum dots with a magnetic moment

To learn what the defects do to the material, the researchers calculated the spin-polarized density of states (DOS), that is, how many electronic states with spin up and spin down exist at each energy (Fig. 7). The defects introduce many states inside the band gap. These are localized around the defects, which therefore scatter electrons and affect transport. In tetravacancies I and II, spin-up and spin-down states are shifted against each other, so the defects become magnetic. While pristine $MoTe_2$ is nonmagnetic[24], the calculations gave a total magnetic moment of 4 μ_B for tetravacancy I and 2 μ_B for tetravacancy II, mainly localized on the three Mo atoms around the central Te atom. Embedded in a semiconducting matrix, such defects can be regarded as quantum dots. A single Te vacancy, by contrast, is hardly spin-polarized, and the trefoil defects are nonmagnetic.

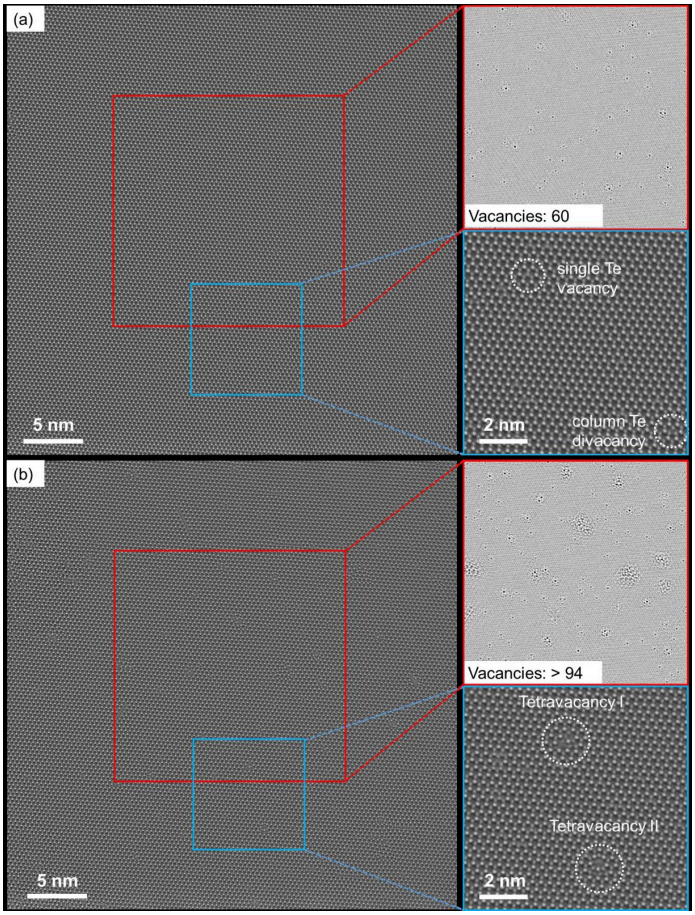

Fig. 2: Dose series of the same area.

"With the combination of first-principles calculations we are explaining the defect formation, migration, and their coalescence resulting ultimately in the formation of inversion domains," said Ute Kaiser, head of the Electron Microscopy Group of Materials Science at Ulm University. "The controllable introduction of particular defects that introduce certain functionalities may be used application-related for devices with new optical, electronic, and magnetic properties."

Vacancy lines as quantum wires

Continued imaging also produced line defects. Fig. 8 compares an experimental image of a single vacancy line with four missing Te atoms with an image calculated from the DFT structure; the best match was found for a sample tilt of 4°, and small differences likely stem from strain around the missing atoms. DFT calculations of various vacancy lines showed that vacancies prefer to line up along the zigzag direction of the lattice rather than the armchair direction (Fig. 9). Along zigzag, the energy released per Te atom is about 0.04 eV for a single vacancy line and 0.6 eV for a staggered divacancy line; along armchair, only the column divacancy line releases energy at all.

"We have a situation where subsequent TEM imaging also results in line defect formation," said Ute Kaiser. "However, also for the extended defects, the comparison of the atom positions between experimental and simulated images today can provide understanding of the properties of the materials."

For dense vacancy lines, the calculated DOS shows new states that act like a reduced band gap (Fig. 10). More importantly, the lines are metallic and confined within the semiconducting sheet, so they can be regarded as quantum wires. The spin-up and spin-down electron densities are localized in space, which suggests that some of these metallic structures, such as the column Te divacancy line, could be used in spintronics.

Lines or clusters: what the energies tell

The formation energies of all observed structures explain how the defects evolve under the beam (Fig. 11). Single Te vacancies gain energy by forming lines, which is why the experiments showed single vacancy lines along zigzag. For column Te divacancies, lines are only slightly favored, but clustering into extended point defects releases a substantial amount of energy. The system therefore forms tetravacancies, via the metastable tetravacancy I, rather than column vacancy lines. The trefoil, with 3.88 eV per Te atom, is strongly preferred over a divacancy line with the same number of missing atoms.

Inversion domains and metallic islands

At higher vacancy concentrations, inversion domains formed after a total dose of about 1.4×10^9 electrons per nm^2, bordered by MTBs of the 4|4P and 4|4E types (Fig. 12a–c). 4|4P boundaries had been reported before after thermal annealing, which also removes Te, but the 4|4E boundary from Te deficiency had never been seen in $MoTe_2$. In another area, the strain of a single vacancy line with six missing Te atoms pushed neighboring Te

atoms aside, and an island of the metallic 1T′ phase appeared within one second, while the vacancy line moved by two unit cells (Fig. 12d–f). Similar transformations had been observed under the electron beam in Re-doped MoS_2[5]; they likely originate from strain induced by vacancies and possibly from charge transfer and vibrational effects[25],[26].

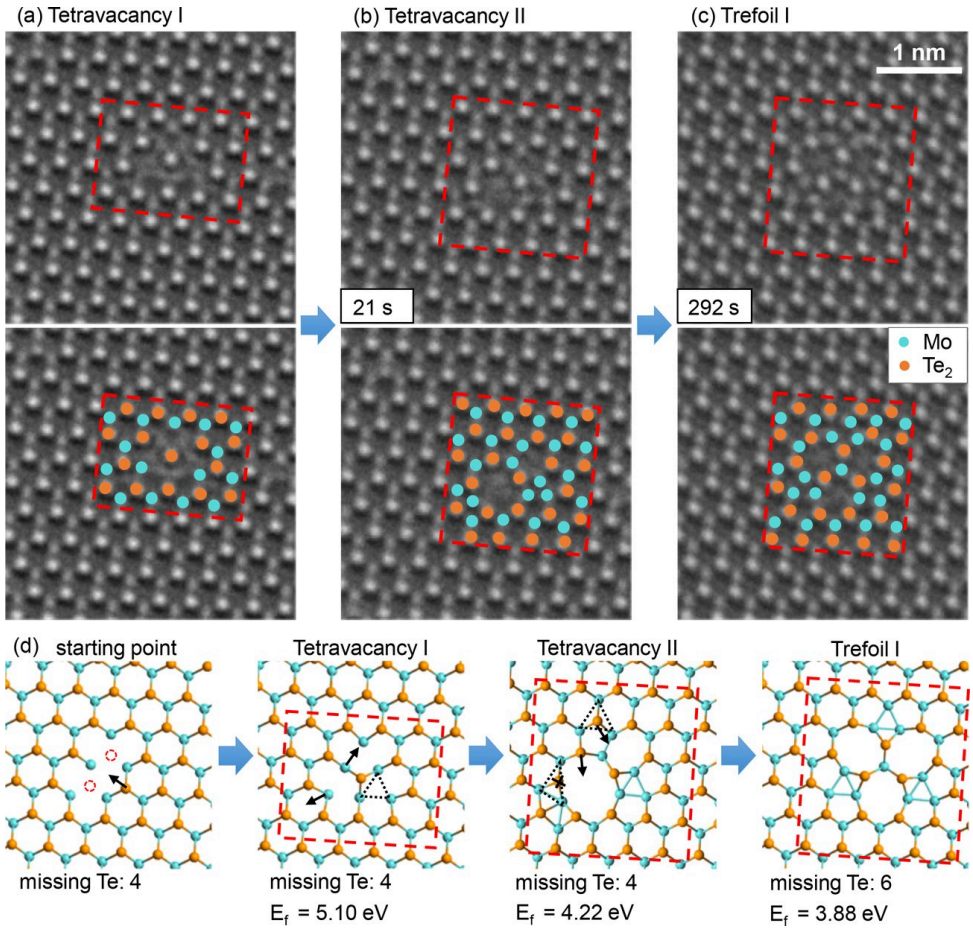

Fig. 3: Tetravacancies and trefoil at 40 kV.

"Finally, using the 40 kV electron beam, we were able to provide insights into the formation and evolution process of inversion domains with mirror twin boundaries of different types, along with the islands of the metallic phases that occur," Kaiser said. The results are also relevant for other TMDs[20],[21],[27],[28], as they relate the atomic structure of the emerging MTBs[16] to the experimental conditions[21],[28]. The calculations behind them are summarized in the box.

DFT: energies, spins and structures

The calculations used density functional theory with the PBE exchange-correlation functional[29] as implemented in the VASP code[30]. Defects were modelled in 10 × 10 supercells of a $MoTe_2$ monolayer, fully relaxed until all forces were below 0.01 eV/Å, with a plane-wave cutoff of 400 eV. Formation energies were calculated relative to the pristine sheet, with the spin-polarized energy of the isolated atom as chemical potential.

The HRTEM image simulations used a focal spread of 0.5 nm, a fifth-order spherical aberration of 1.8 mm, a defocus of 7.5 nm and a third-order spherical aberration of −8.2 µm, as optimized for the experimental images.

What it opens up

The study showed a plethora of point and line defects in monolayer $MoTe_2$ and how they form, migrate and coalesce. Metallic islands of the T′ phase can act as quantum dots, while vacancy lines and mirror twin boundaries form one-dimensional metallic systems embedded in a semiconductor. "The latter structure is very interesting in the context of fundamental aspects of the physics of Tomonaga–Luttinger liquid and, as for practical aspects, plasmonics," the authors write. Together with the defect-associated magnetism, this opens a route towards quantum devices made by defect engineering in single-layer $MoTe_2$.

"We showed that some of the observed defects have localized magnetic moments," Kaiser said. "This may lead toward control of optical and electronic properties for quantum devices in 2D materials. Other systems that we observed are very interesting in the context of fundamental aspects of physics and for practical aspects in plasmonics."

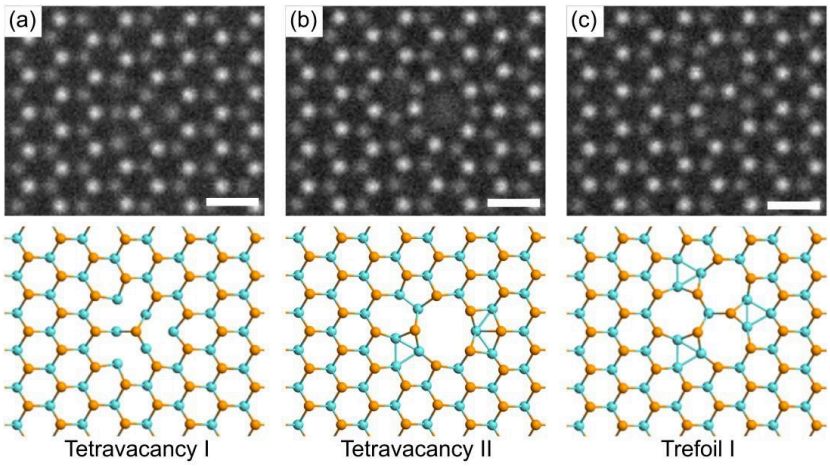

Fig. 4: Simulated images of the defects.

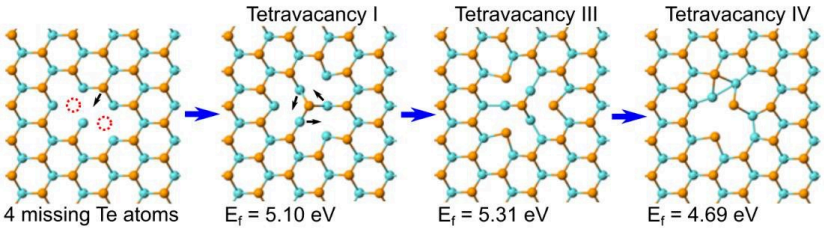

Fig. 5: Rotated tetravacancy variants.

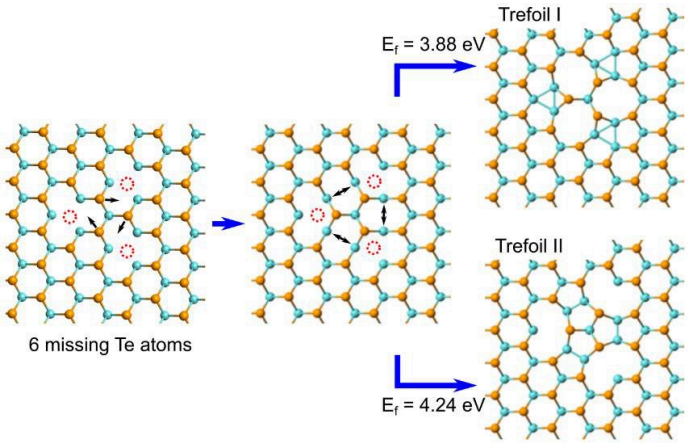

Fig. 6: Trefoil variants in DFT.

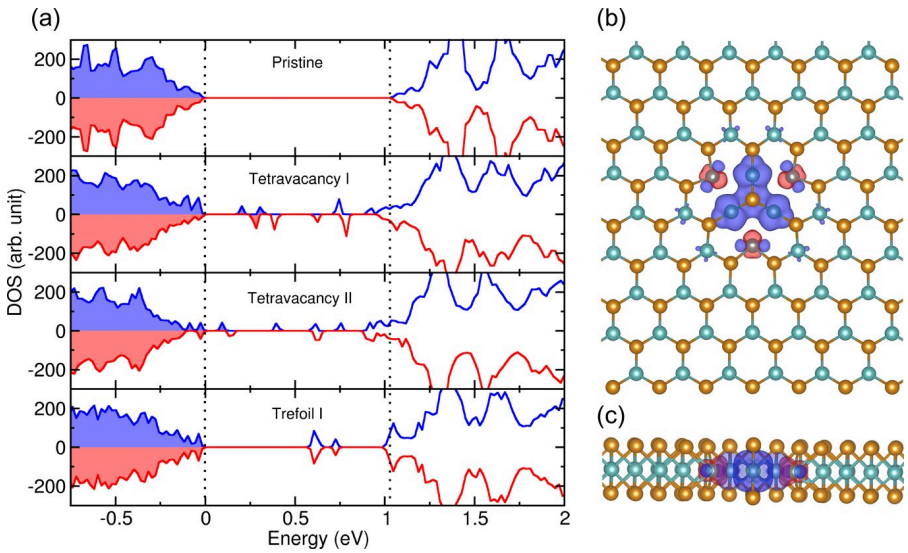

Fig. 7: Density of states and spin density.

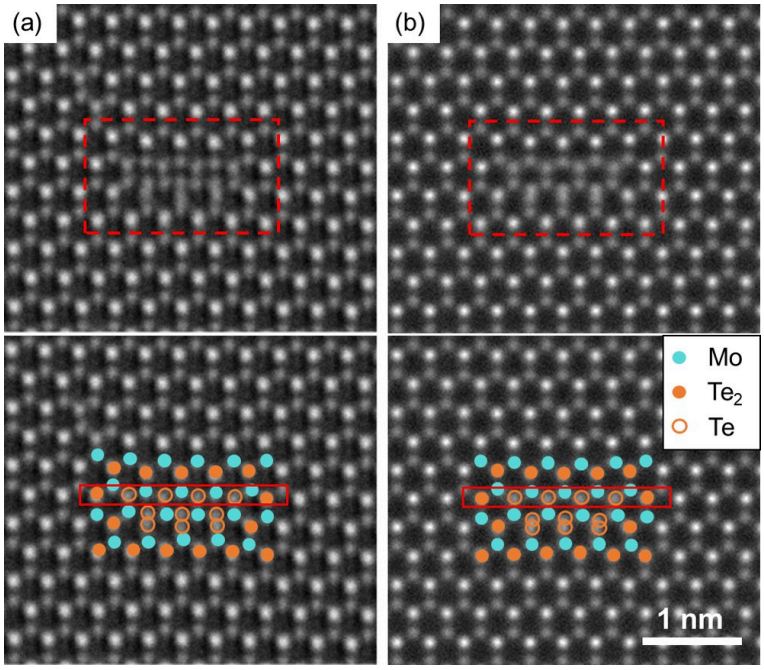

Fig. 8: Vacancy line: experiment and simulation.

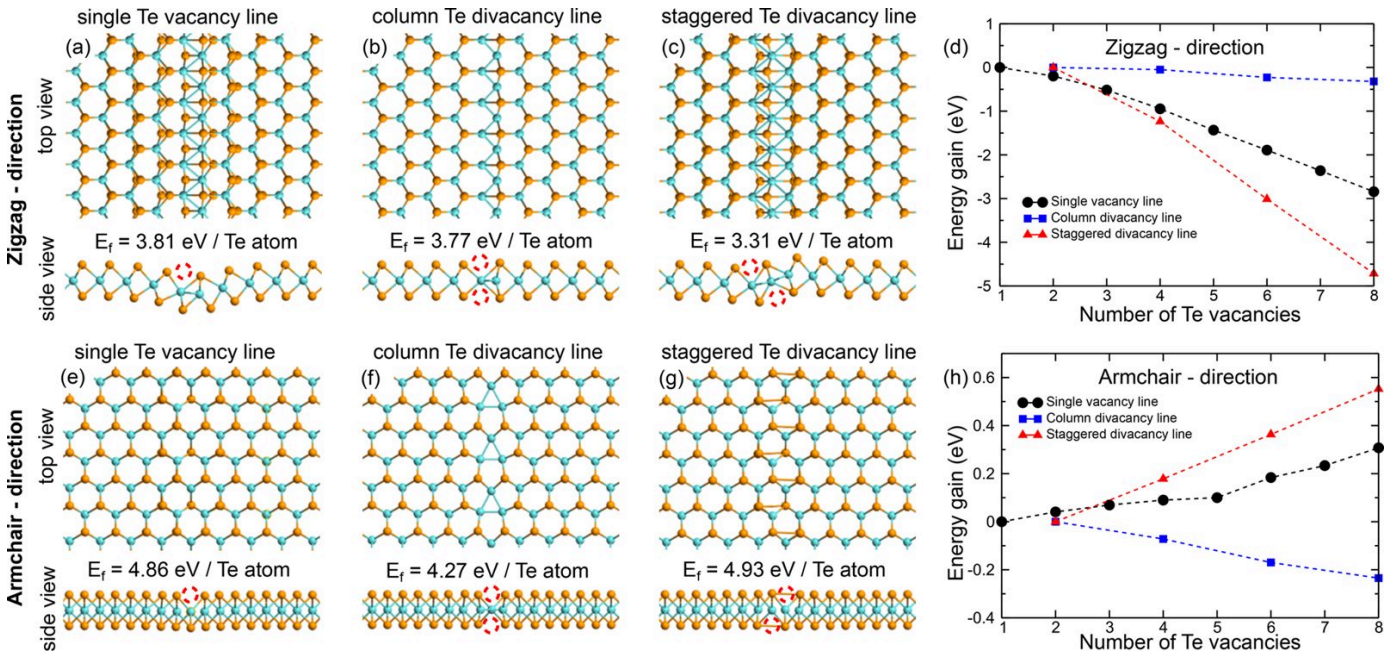

Fig. 9: Vacancy lines along zigzag and armchair.

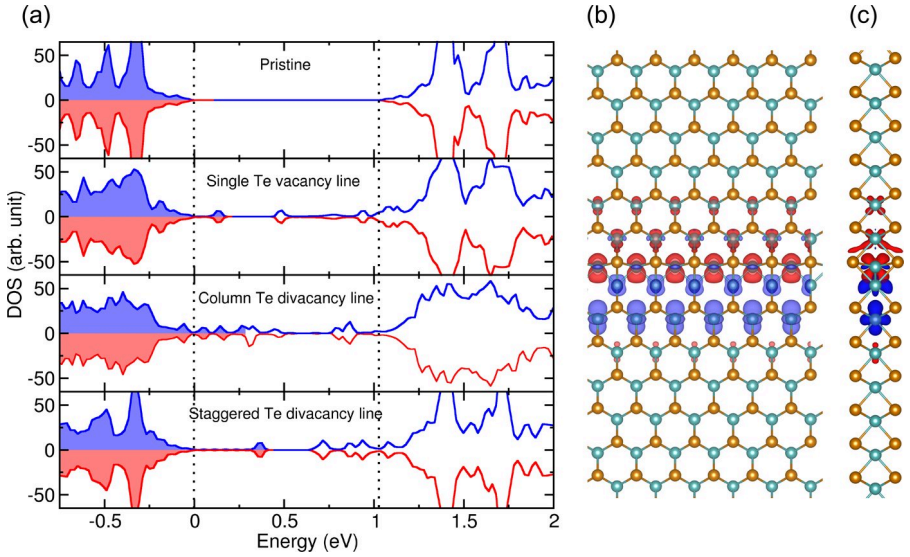

Fig. 10: Density of states of vacancy lines.

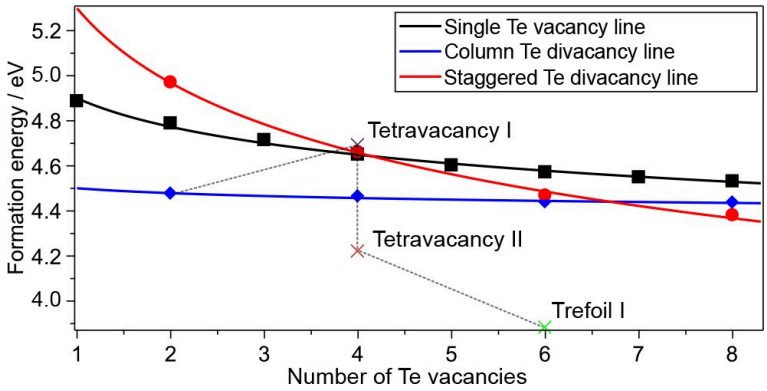

Fig. 11: Energies of lines and clusters.

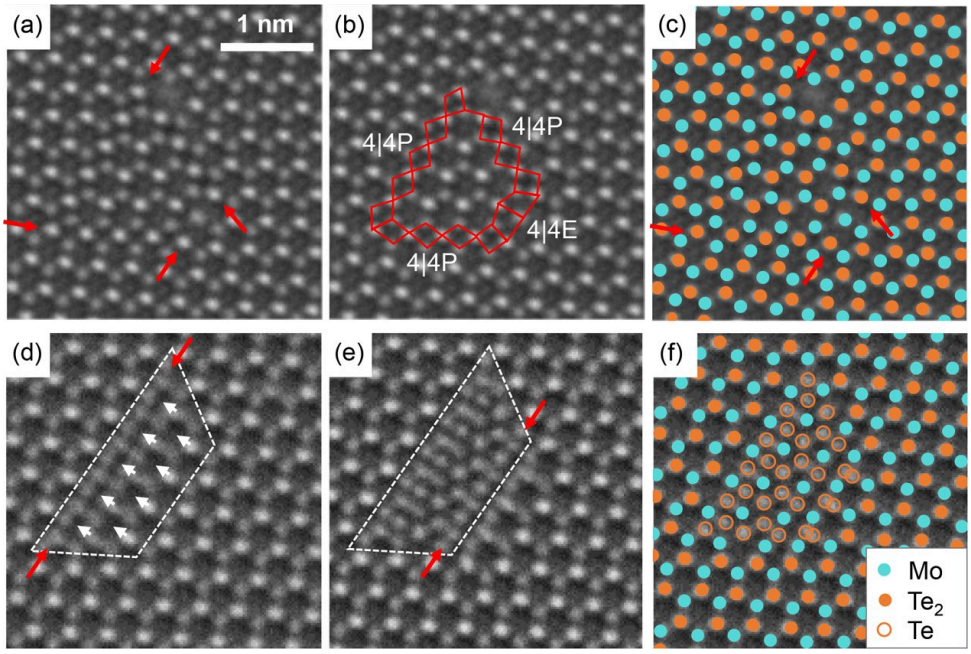

Fig. 12: Mirror twin boundaries and 1T′ phase.

Resource

Lehnert, T., Ghorbani-Asl, M., Köster, J., Lee, Z., Krasheninnikov, A. V., Kaiser, U. (2019). Electron-Beam-Driven Structure Evolution of Single-Layer $MoTe_2$ for Quantum Devices.

ACS Appl. Nano Mater. **2**(5), 3262–3270.
https://doi.org/10.1021/acsanm.9b00616

References

1. Kaiser, U., Biskupek, J., Meyer, J. C., Leschner, J., Lechner, L., Rose, H., Stöger-Pollach, M., Khlobystov, A. N., Hartel, P., Müller, H., Haider, M., Eyhusen, S., Benner, G. (2011). Transmission electron microscopy at 20 kV for imaging and spectroscopy. *Ultramicroscopy*, **111**, 1239–1246. https://doi.org/10.1016/j.ultramic.2011.03.012
2. Linck, M., Hartel, P., Uhlemann, S., Kahl, F., Müller, H., Zach, J., Haider, M., Niestadt, M., Bischoff, M., Biskupek, J., Lee, Z., Lehnert, T., Börrnert, F., Rose, H., Kaiser, U. (2016). Chromatic Aberration Correction for Atomic Resolution TEM Imaging from 20 to 80 kV. *Phys. Rev. Lett.*, **117**, 076101. https://doi.org/10.1103/physrevlett.117.076101
3. Lee, Z., Meyer, J. C., Rose, H., Kaiser, U. (2012). Optimum HRTEM image contrast at 20 kV and 80 kV—Exemplified by graphene. *Ultramicroscopy*, **112**, 39–46. https://doi.org/10.1016/j.ultramic.2011.10.009
4. Chhowalla, M., Shin, H. S., Eda, G., Li, L.-J., Loh, K. P., Zhang, H. (2013). The chemistry of two-dimensional layered transition metal dichalcogenide nanosheets. *Nat. Chem.*, **5**, 263–275. https://doi.org/10.1038/nchem.1589
5. Lin, Y.-C., Dumcenco, D. O., Huang, Y.-S., Suenaga, K. (2014). Atomic mechanism of the semiconducting-to-metallic phase transition in single-layered MoS_2. *Nat. Nanotechnol.*, **9**, 391–396. https://doi.org/10.1038/nnano.2014.64
6. Wilson, J. A., Di Salvo, F. J., Mahajan, S. (1975). Charge-density waves and superlattices in the metallic layered transition metal dichalcogenides. *Adv. Phys.*, **24**, 117–201. https://doi.org/10.1080/00018737500101391
7. Wang, Q. H., Kalantar-Zadeh, K., Kis, A., Coleman, J. N., Strano, M. S. (2012). Electronics and optoelectronics of two-dimensional transition metal dichalcogenides. *Nat. Nanotechnol.*, **7**, 699–712. https://doi.org/10.1038/nnano.2012.193
8. Deng, K., Wan, G., Deng, P., Zhang, K., Ding, S., Wang, E., Yan, M., Huang, H., Zhang, H., Xu, Z., Denlinger, J., Fedorov, A., Yang, H., Duan, W., Yao, H., Wu, Y., Fan, S., Zhang, H., Chen, X., Zhou, S. (2016). Experimental observation of topological Fermi arcs in type-II Weyl semimetal $MoTe_2$. *Nat. Phys.*, **12**, 1105–1110. https://doi.org/10.1038/nphys3871
9. Zhao, X., Kotakoski, J., Meyer, J. C., Sutter, E., Sutter, P., Krasheninnikov, A. V., Kaiser, U., Zhou, W. (2017). Engineering and modifying two-dimensional materials by electron beams. *MRS Bull.*, **42**, 667–676. https://doi.org/10.1557/mrs.2017.184
10. Kalinin, S. V., Pennycook, S. J. (2017). Single-atom fabrication with electron and ion beams: From surfaces and two-dimensional materials toward three-dimensional atom-by-atom assembly. *MRS Bull.*, **42**, 637–643. https://doi.org/10.1557/mrs.2017.186
11. Susi, T., Meyer, J. C., Kotakoski, J. (2017). Manipulating low-dimensional materials down to the level of single atoms with electron irradiation. *Ultramicroscopy*, **180**, 163–172. https://doi.org/10.1016/j.ultramic.2017.03.005
12. Susi, T., Meyer, J. C., Kotakoski, J. (2019). Quantifying transmission electron microscopy irradiation effects using two-dimensional materials. *Nat. Rev. Phys.*, **1**, 397–405. https://doi.org/10.1038/s42254-019-0058-y
13. Dyck, O., Ziatdinov, M., Lingerfelt, D. B., Unocic, R. R., Hudak, B. M., Lupini, A. R., Jesse, S., Kalinin, S. V. (2019). Atom-by-atom fabrication with electron beams. *Nat. Rev. Mater.*, **4**, 497–507. https://doi.org/10.1038/s41578-019-0118-z
14. Cho, S., Kim, S., Kim, J. H., Zhao, J., Seok, J., Keum, D. H., Baik, J., Choe, D.-H., Chang, K. J., Suenaga, K., Kim, S. W., Lee, Y. H., Yang, H. (2015). Phase patterning for ohmic homojunction contact in $MoTe_2$. *Science*, **349**, 625–628. https://doi.org/10.1126/science.aab3175
15. Kosmala, T., Coy Diaz, H., Komsa, H.-P., Ma, Y., Krasheninnikov, A. V., Batzill, M., Agnoli, S. (2018). Metallic Twin Boundaries Boost the Hydrogen Evolution Reaction on the Basal Plane of Molybdenum Selenotellurides. *Adv. Energy Mater.*, **8**, 1800031. https://doi.org/10.1002/aenm.201800031
16. Komsa, H.-P., Krasheninnikov, A. V. (2017). Engineering the Electronic Properties of Two-Dimensional Transition Metal Dichalcogenides by Introducing Mirror Twin Boundaries. *Adv. Electron. Mater.*, **3**, 1600468. https://doi.org/10.1002/aelm.201600468

17. Ma, Y., Kolekar, S., Coy Diaz, H., Aprojanz, J., Miccoli, I., Tegenkamp, C., Batzill, M. (2017). Metallic Twin Grain Boundaries Embedded in $MoSe_2$ Monolayers Grown by Molecular Beam Epitaxy. *ACS Nano*, **11**, 5130–5139. https://doi.org/10.1021/acsnano.7b02172

18. Lehtinen, O., Komsa, H.-P., Pulkin, A., Whitwick, M. B., Chen, M.-W., Lehnert, T., Mohn, M. J., Yazyev, O. V., Kis, A., Kaiser, U., Krasheninnikov, A. V. (2015). Atomic Scale Microstructure and Properties of Se-Deficient Two-Dimensional $MoSe_2$. *ACS Nano*, **9**, 3274–3283. https://doi.org/10.1021/acsnano.5b00410

19. Barja, S., Wickenburg, S., Liu, Z.-F., Zhang, Y., Ryu, H., Ugeda, M. M., Hussain, Z., Shen, Z.-X., Mo, S.-K., Wong, E., Salmeron, M. B., Wang, F., Crommie, M. F., Ogletree, D. F., Neaton, J. B., Weber-Bargioni, A. (2016). Charge density wave order in 1D mirror twin boundaries of single-layer $MoSe_2$. *Nat. Phys.*, **12**, 751–756. https://doi.org/10.1038/nphys3730

20. Algara-Siller, G., Kurasch, S., Sedighi, M., Lehtinen, O., Kaiser, U. (2013). The pristine atomic structure of MoS_2 monolayer protected from electron radiation damage by graphene. *Appl. Phys. Lett.*, **103**, 203107. https://doi.org/10.1063/1.4830036

21. Wang, S., Lee, G.-D., Lee, S., Yoon, E., Warner, J. H. (2016). Detailed Atomic Reconstruction of Extended Line Defects in Monolayer MoS_2. *ACS Nano*, **10**, 5419–5430. https://doi.org/10.1021/acsnano.6b01673

22. Komsa, H.-P., Kotakoski, J., Kurasch, S., Lehtinen, O., Kaiser, U., Krasheninnikov, A. V. (2012). Two-Dimensional Transition Metal Dichalcogenides under Electron Irradiation: Defect Production and Doping. *Phys. Rev. Lett.*, **109**, 035503. https://doi.org/10.1103/physrevlett.109.035503

23. Meyer, J. C., Eder, F., Kurasch, S., Skakalova, V., Kotakoski, J., Park, H. J., Roth, S., Chuvilin, A., Eyhusen, S., Benner, G., Krasheninnikov, A. V., Kaiser, U. (2012). Accurate Measurement of Electron Beam Induced Displacement Cross Sections for Single-Layer Graphene. *Phys. Rev. Lett.*, **108**, 196102. https://doi.org/10.1103/physrevlett.108.196102

24. Ataca, C., Sahin, H., Akturk, E., Ciraci, S. (2011). Mechanical and Electronic Properties of MoS_2 Nanoribbons and Their Defects. *J. Phys. Chem. C*, **115**, 3934–3941. https://doi.org/10.1021/jp1115146

25. Duerloo, K.-A. N., Li, Y., Reed, E. J. (2014). Structural phase transitions in two-dimensional Mo- and W-dichalcogenide monolayers. *Nat. Commun.*, **5**, 4214. https://doi.org/10.1038/ncomms5214

26. Kretschmer, S., Komsa, H.-P., Bøggild, P., Krasheninnikov, A. V. (2017). Structural Transformations in Two-Dimensional Transition-Metal Dichalcogenide MoS_2 under an Electron Beam: Insights from First-Principles Calculations. *J. Phys. Chem. Lett.*, **8**, 3061–3067. https://doi.org/10.1021/acs.jpclett.7b01177

27. Pizzochero, M., Yazyev, O. V. (2017). Point defects in the 1T′ and 2H phases of single-layer MoS_2: A comparative first-principles study. *Phys. Rev. B*, **96**, 245402. https://doi.org/10.1103/physrevb.96.245402

28. Komsa, H.-P., Kurasch, S., Lehtinen, O., Kaiser, U., Krasheninnikov, A. V. (2013). From point to extended defects in two-dimensional MoS_2: Evolution of atomic structure under electron irradiation. *Phys. Rev. B*, **88**, 035301. https://doi.org/10.1103/physrevb.88.035301

29. Perdew, J. P., Burke, K., Ernzerhof, M. (1996). Generalized Gradient Approximation Made Simple. *Phys. Rev. Lett.*, **77**, 3865–3868. https://doi.org/10.1103/physrevlett.77.3865

30. Kresse, G., Furthmüller, J. (1996). Efficiency of ab-initio total energy calculations for metals and semiconductors using a plane-wave basis set. *Comput. Mater. Sci.*, **6**, 15–50. https://doi.org/10.1016/0927-0256(96)00008-0